J Mater Sci (2010) 45:5332–5338
DOI 10.1007/s10853-010-4581-6

Microstructure and mechanical property of the fusion boundary region in an Alloy 182-low alloy steel dissimilar weld joint

J. Hou · Q. J. Peng · Y. Takeda · J. Kuniya · T. Shoji · J. Q. Wang · E.-H. Han · W. Ke

Received: 28 January 2010 / Accepted: 28 April 2010 / Published online: 14 May 2010

Abstract Characterizations of the microstructure and mechanical property of the fusion boundary region of an Alloy 182-A533B low alloy steel (LAS) dissimilar weld joint were conducted. The existence of type-II boundary that parallels to the fusion boundary in the dilution zone (DZ) of Alloy 182 within a distance of about 50 μm was observed. The chemical composition transition was found in the narrow zone between the type-II and the fusion boundaries. Highest hardness was also found in this narrow zone in the fusion boundary region, implying a high residual strain level in the narrow zone. Lath martensite was observed in both sides of the type-II boundary in DZ, suggesting the localized enrichment of Fe and C adjacent to the type-II boundary due to the diffusion from LAS to DZ. Massive precipitations of carbides were observed on the type-II boundary but not on the fusion boundary. In addition, the orientation relationship at the fusion boundary between the lath martensite in the heat-affected zone in LAS and the austenite in the DZ was found to be Bain, K–S and N–W relationships.

J. Hou · Q. J. Peng (✉) · Y. Takeda · J. Kuniya · T. Shoji
Fracture and Reliability Research Institute, Graduate School of Engineering, Tohoku University, 6-6-01, Aramaki Aoba, Aoba-ku, Sendai 980-8579, Japan
e-mail: qpeng@rift.mech.tohoku.ac.jp

J. Hou · J. Q. Wang · E.-H. Han · W. Ke
State Key of Laboratory for Corrosion and Protection, Institute of Metal Research, Chinese Academy of Sciences, 62 Wencui Road, 110016 Shenyang, China

Introduction

Alloy 182 is used frequently as filler metal in the manufacture of dissimilar metal welds (DMWs) in light water reactors (LWR) to join the low alloy steel (LAS) pressure vessel nozzles and steam generator nozzles to nickel-base wrought alloy or austenitic stainless steel components. The thermal expansion coefficient of the alloy lies between those of ferritic steel and austenitic stainless steel, and it also significantly retards the carbon diffusion from the ferritic base metal to the weld metal [1]. However, in recent years a concern has been raised about the integrity of the Alloy 182-LAS DMW joint due to the high susceptibility of Alloy 182 to stress corrosion cracking (SCC) in the environments of LWR [2–4].

The DMW has some uniquenesses in its microstructure [5–10]. The first uniqueness is the composition gradient from the base metal to the weld metal across the fusion boundary. Such a change of the composition causes the change in the microstructure, mechanical property as well as the corrosion resistance. The second uniqueness is the change of crystal microstructure from B.C.C., ferritic base metal to F.C.C., austenitic weld metal. This in turn affects the mechanical property of the joint across the fusion boundary and may result in the formation of type-II boundary that parallels to the fusion boundary in the weld metal within a distance of <100 μm [10–13]. The third uniqueness is the formation of residual stress in the fusion boundary region due to the microstructure heterogeneity and the resultant thermal mismatch, which results in the gradient of mechanical properties across the fusion boundary [14, 15].

Since the material microstructure is a key parameter affecting the SCC, improving the understanding of SCC at the fusion boundary region requires fundamental

understanding of the unique microstructure of the fusion boundary region. Nelson et al. [12, 13] found that the fusion boundary exhibited random misorientations between base and weld metal grains in a dissimilar weld joint of 409 stainless steel-AISI 1080 alloy. They also concluded that the type-II boundary was a potential path for cracking and had been formed as a result of the occurrence of the allotropic δ–γ transformation at elevated temperatures. Research of mechanical properties of the fusion boundary region of dissimilar weld joints showed that highest hardness existed near the fusion boundary while the heat-affected zone (HAZ) in LAS showed higher hardness than the base metal. The hardness in the dilution zone (DZ) of the weld metal, however, did not show obvious difference with the weld metal [16, 17].

While works have been conducted on the microstructure of the fusion boundary region of a DMW, there still lack of understanding of the microstructure of the fusion boundary region. In particular, to the author's knowledge, detailed microstructure of the narrow zone between the fusion boundary and type-II boundary, and the mechanical property of the narrow zone need further investigations. Further, no such works have been done on Alloy 182-LAS DMW. The objectives of this study are to clarify the microstructure of the fusion boundary region in an Alloy 182-LAS dissimilar weld joint with focuses on the narrow zone between the fusion boundary and the type-II boundary, and the mechanical property in HAZ and DZ.

Experiment

Materials and specimen

The weld joint of Alloy 182-A533-B LAS was prepared by multipass shielded metal arc welding (SMAW) followed by post-welding heat treatment (PWHT) at 615 °C for 25 h with air cooling to relieve the residual stress. Chemical compositions of both metals were shown in Table 1. Specimens were cut from the dissimilar weld joint (Fig. 1).

Microstructure characterization

Metallographic microstructure of the fusion boundary region was characterized by optical microscopy and scanning electron microscopy (SEM) following etching the specimen using a solution of $CuCl_2{\cdot}2H_2O$ (10 g) + HCl (50 mL) + ethonal (50 mL). Chemical composition in the fusion boundary region was analyzed by SEM-energy-dispersive X-ray (EDX) spectroscopy.

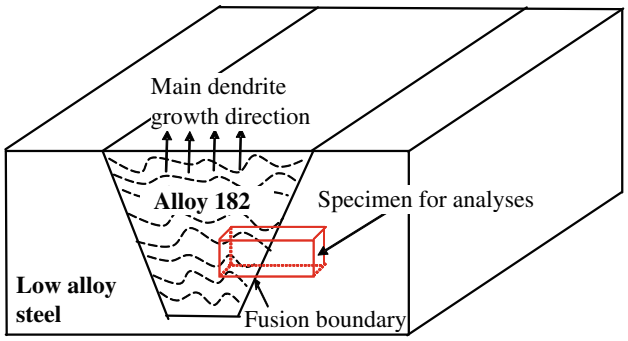

Fig. 1 Schematic drawing showing the extraction of the samples for the analysis from the dissimilar metal weld joint

The grain boundary misorientation at the fusion boundary and the orientations of martensite in HAZ were analyzed using electron backscatter diffraction (EBSD) conducted by a Hitachi 4300 SEM equipped with a TSL Laboratories Orientation Imaging Microscope system at an accelerate voltage of 25 kV. The specimens for EBSD examination were ground by emery papers up to 4000 grit, then polished by diamond paste to 0.25 μm, and finally polished by 0.02 μm colloidal silica for 1 h that provided flat surfaces with little surface deformation.

A Hitachi HF-2000 transmission electronic microscopy (TEM) was used for analyzing the transition of crystallographic microstructure and chemical composition in the fusion boundary region, and the precipitation at type-II and fusion boundaries. For the preparation of the TEM specimens, a plate of 1-mm thick, 4-mm long, and 4-mm wide containing either the fusion boundary or the type-II boundary were cut using a dicing saw from a block of the dissimilar weld joint. Then the small pieces were polished and etched before they were transferred to a Hitachi FB200A Focused Ion Beam (FIB) system for thinning. Locations of interests containing the fusion boundary or type-II boundary were identified using the scanning ion microscope attached with the FIB system. Then they were deposited by tungsten, followed by rough cutting, and fine thinning by Ga ion with different beam currents to obtain a

Table 1 Chemical compositions of base and weld metals (wt%)

Element	C	Si	Mn	P	S	Cu	Ni	Cr	Mo	V	Nb + Ta	Nb	Ti	Fe
A533Gr.B	0.20	0.24	1.42	0.01	0.006	0.11	0.64	0.12	0.54	0.003		0.002	0.001	Bal.
Alloy 182	0.053	0.44	6.50	0.004	0.002		68.90	14.7			1.55	1.50		7.23

specimen thickness of less than 100 nm. An accelerated beam voltage of 200 kV was used for the TEM analyses.

Mechanical property characterization

The mechanical properties of the base metal, weld metal, HAZ, and DZ of the dissimilar weld joint at 288 °C were measured by a series of tensile tests on cylindrical tensile specimens. Two types of tensile specimens were employed: small-sized specimen with a diameter of 1.5 mm and a gage length of 5.3 mm, and big-sized specimens machined according to the Japanese Industrial Standard (JIS). The small-sized specimens were used to measure the local mechanical properties of the DZ in weld metal and HAZ in base metal near the fusion boundary, while the JIS specimens were used to measure the mechanical properties of the base and weld metals, as well as to confirm the reliability of the data obtained from the small-sized specimens. Locations of the tensile specimens in the dissimilar weld joint were schematically shown in Fig. 2.

Micro-hardness profile of the fusion boundary region was measured using a Shimadzu-Hmv micro-hardness tester. The load and holding time used for the measurement is 25 g and 20 S, respectively.

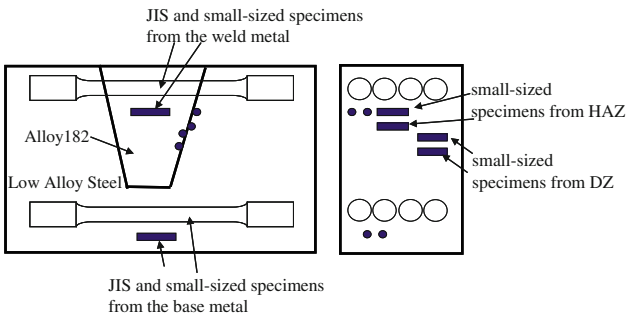

Fig. 2 Schematic drawings showing the extraction of the JIS and small-sized tensile specimens from the dissimilar metal weld joint. The *open circle* denotes the JIS specimen, and the *full circle* denotes the small-sized specimen

Results and discussion

Microstructure of the fusion boundary region observed by SEM

The DZ in Alloy 182 is composed of columnar grains that are similar to the weld metal (Fig. 3a). Unmixed-zone in the DZ was observed near the fusion boundary (Fig. 3b). It is noted that type-II boundary was observed in Fig. 3a, which is parallel to the fusion boundary in the DZ with a distance of about 50 μm. The type-II boundary was hypothesized to be formed as a result of a change in the primary mode solidification [12, 13]. The microstructure from the fusion boundary to HAZ in LAS is shown in Fig. 4a–d. As can be seen, large grains consist of lath martensite exist near the fusion boundary. With increasing the distance from the fusion boundary, the grain size gradually decreases and is saturated at a distance of about 0.6 mm. In addition, the lath martensite starts to disappear at a distance of about 0.4 mm. At a distance of 0.6 mm, only α-ferrite and colloidal carbides were observed that is similar to the microstructure of the base metal.

Composition profile of the fusion boundary region

Figure 5a shows the composition profile from the base metal to weld metal measured by SEM-EDX. The DZ has a width of about 2 mm containing lower Ni and Cr but higher Fe than the weld metal. Composition profile of the narrow zone between the fusion boundary and the type-II boundary analyzed at a higher magnification is shown in Fig. 5b. A deep decrease of Fe and increase of Ni was observed in the narrow zone within a distance of 20–30 μm from the fusion boundary. The deep gradient of the

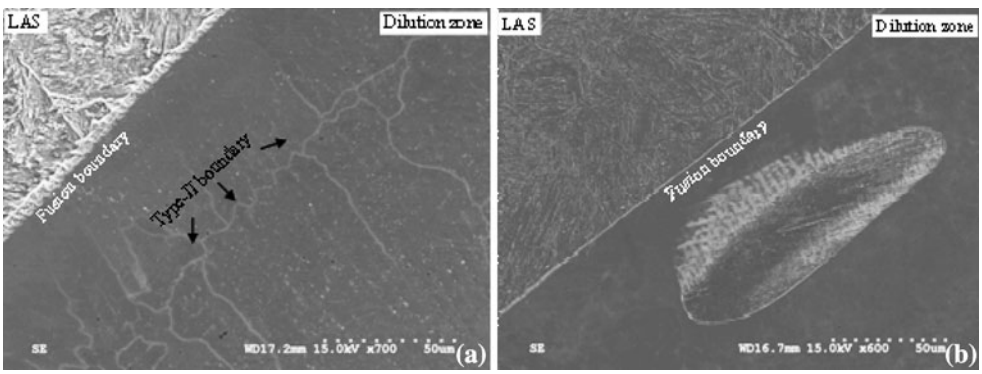

Fig. 3 SEM observations showing the columnar grains and type-II boundary (**a**) and the unmixed zone (**b**) in the DZ

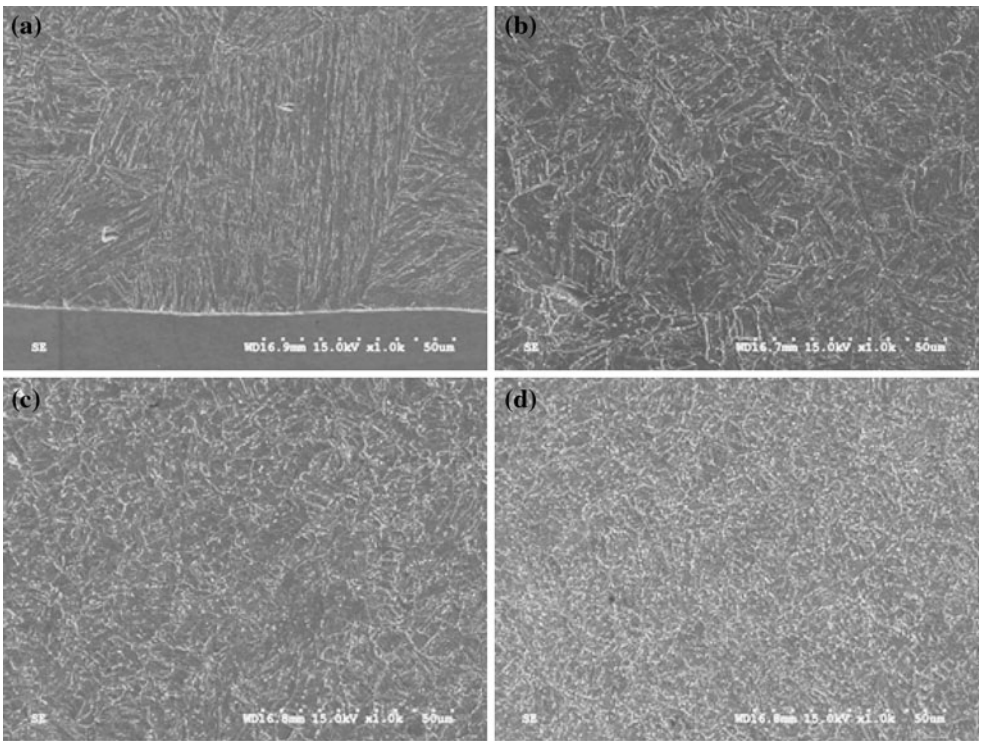

Fig. 4 SEM pictures showing the change in the microstructure from the fusion boundary to HAZ in the base metal. **a** Near the fusion boundary, **b** ~0.2 mm from the fusion boundary, **c** ~0.4 mm from the fusion boundary, **d** ~0.6 mm from the fusion boundary

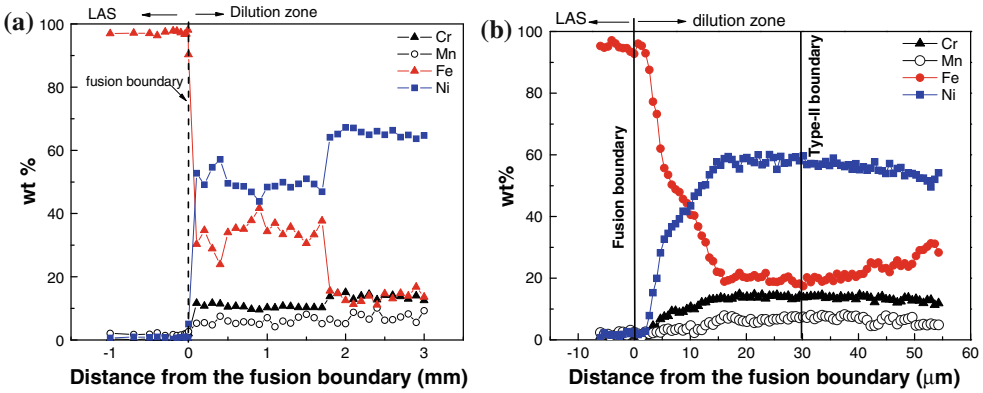

Fig. 5 The composition profiles in the DMW measured by SEM-EDX. **a** The profile from the base metal to weld metal, and **b** the profile of the narrow zone from the fusion boundary to the type-II boundary

chemical composition in the narrow zone may generate high residual strain and high hardness.

Hardness and mechanical property of the fusion boundary region

Typical hardness profile from the HAZ to the DZ is shown in Fig. 6a. The hardness of the base and weld metals is similar. As can be expected, the HAZ shows a hardness of about 50HV higher than the base metal. However, the hardness of the DZ is approximately equal to the weld metal. The hardness in DZ adjacent to the fusion boundary is much higher than those of HAZ and other locations of DZ (Fig. 6b). The locations show highest hardness was found to be in the narrow zone between the type-II boundary and the fusion boundary. This is demonstrated by the indentations shown in Fig. 7. The hardness increases quickly when the indentations approach to the narrow zone across the type-II boundary in the DZ. This result suggests that the residual strain in the narrow zone is likely the highest in the fusion boundary region, which may be a result of the deep composition change in the narrow zone as mentioned previously.

Figure 8 shows the yield strength of the base metal, HAZ, DZ, and the weld metal measured at 288 °C. The yield strength of the HAZ is at 470–506 MPa, which is

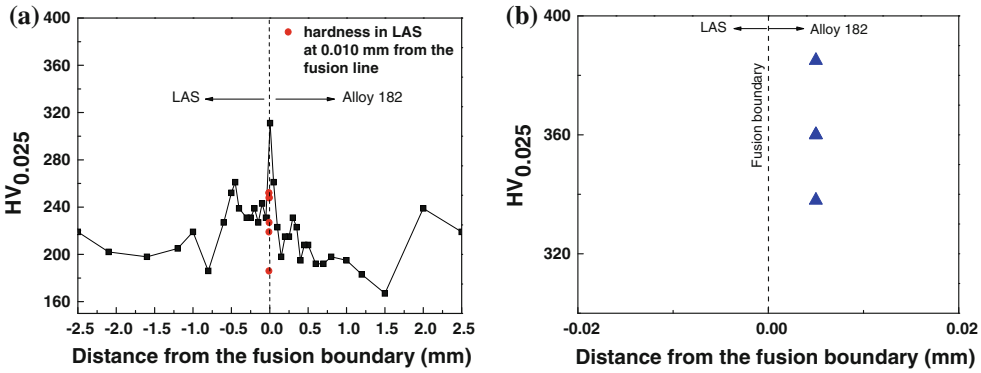

Fig. 6 The micro-hardness profile of the fusion boundary region (**a**), and the micro-hardness in the dilution zone at locations of 0.005 mm from the fusion boundary (**b**)

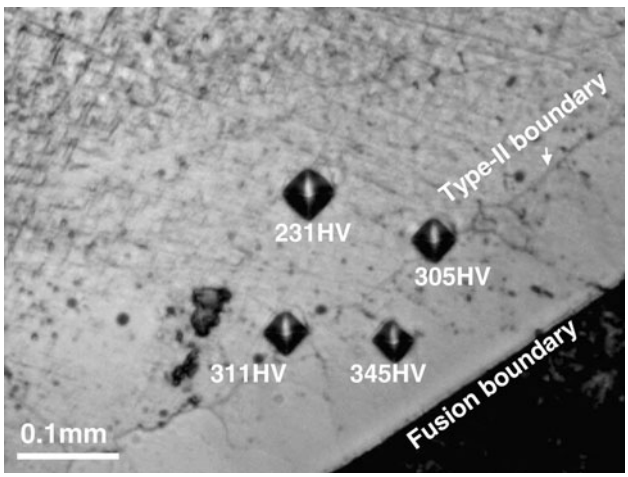

Fig. 7 Indentations in the DZ, adjacent to the type-II boundary and in the narrow zone between the type-II and the fusion boundaries that demonstrate the change of the hardness across the type-II boundary

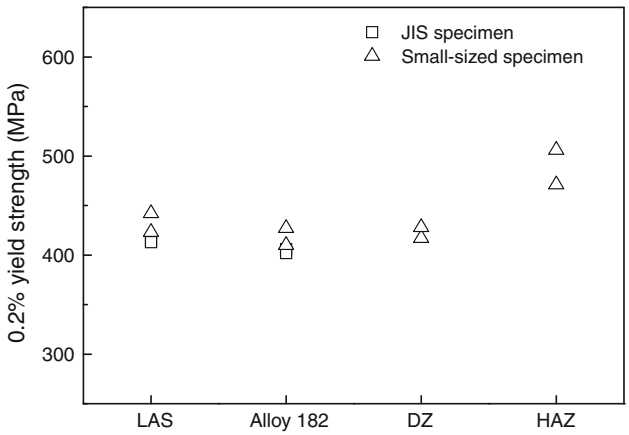

Fig. 8 The yield strength of the base metal, weld metal, DZ, and HAZ in the DMW

about 50–100 MPa higher than those of the base and the weld metals and DZ. This result is compatible with the hardness profile shown in Fig. 6a. However, the highest hardness observed adjacent to the fusion boundary in the DZ did not cause an increase of the measured yield strength of the DZ, indicating that the small-sized specimen is still insufficient to characterize the localized hardening adjacent to the fusion boundary. In addition, the strengths of the base and the weld metals from the small-sized and JIS specimens show little difference, indicating the reliability of the small-sized specimens for measuring the mechanical properties.

The misorientation relationship at the fusion boundary and the misorientation of martensite in the HAZ

In order for clarifying the misorientation of grains at the fusion boundary, a series of pairs of points adjacent to the fusion boundary in both the DZ and the HAZ sides were analyzed by EBSD. The two points for each pair are in the HZ side and the DZ side, respectively. Figure 9a shows the

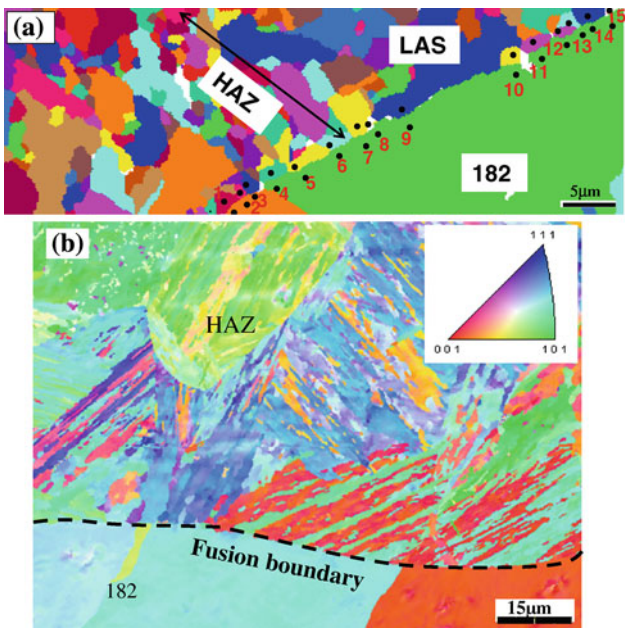

Fig. 9 The orientation maps of the fusion boundary region collected by SEM-EBSD. **a** the *black spots* showing the pairs of points adjacent to the fusion boundary in both DZ and HAZ sides that were analyzed by EBSD and **b** the orientation map of the HAZ near the fusion boundary that shows the blocks of laths of the martensite

Table 2 The misorientation relationships between the pairs of points adjacent to the fusion boundary shown in Fig. 9a

Point	Misorientation	⟨uvw⟩	Relationship
1	48.9	−10−1	N–W
2	39.4	−100	
3	41.8	001	Bain
4	40.1	00−1	Bain
5	43.2	001	Bain
6	45.8	010	Bain
7	38.6	−101	K–S
8	56.2	−101	
9	41.3	0−10	Bain
10	35.6	111	
11	26.5	100	
12	42.2	−1−10	N–W
13	25.7	100	
14	45.1	00−1	Bain
15	46.9	011	N–W

pairs of the points for the EBSD analysis that are marked as black spots. The calculated misorientation relationships between the points as listed in Table 2 shows that there are three kinds of relationships with approximately 45° at ⟨110⟩, 45° at ⟨100⟩, and 35° at ⟨110⟩. These relationships are defined as preferred orientation of N–W, Bain, and K–S relationships [18]. Therefore, during the welding process the growth of austenites and lath martensites adjacent to the fusion boundary were with preferred orientations. Laths of the martensites with similar orientation near the fusion boundary in the HAZ were observed, which are in the same color in the orientation map (Fig. 9b). These laths are most likely from the blocks in packets (the group of laths with same habit plane) in the parent austenite [19–22]. While the misorientation maps of the whole HAZ are not given here, the blocks in HAZ as observed by EBSD are bigger in the regions within a distance of about 300 μm to the fusion boundary. With increasing the distance further from the fusion boundary, the blocks were finer and more degenerate, while the presence of laths with same orientation was still recognizable. This result is in consistence with the SEM observation of the HAZ shown in Fig. 4. The change in the block size with increasing the distance from the fusion boundary is likely due to the decrease of carbon concentration that could reduce the block size [19, 23].

TEM observation of microstructure of fusion and type-II boundaries

The TEM observation of the type-II boundary region adjacent to the fusion boundary in DZ is shown in Fig. 10a and b with different magnifications. The diffraction pattern shown in Fig. 10a indicates the existence of grains with B.C.C. structure adjacent to the type-II boundary. The lath morphology of the B.C.C. grains suggests they are martensite [19, 24, 25]. The lath martensite was observed in both sides of the type-II boundary in DZ, suggesting the localized enrichment of Fe and C in DZ due to the diffusion from LAS to DZ. Discontinuous precipitates were observed along the type-II boundary (Fig. 10b). The diffraction patterns and EDX analyses indicate that the dominant precipitates are composited carbides of Ti and Nb. In addition, precipitation of $Cr_{23}C_6$ at the type-II boundary was also observed (Fig. 10a).

Figure 11 shows the TEM observation of the fusion boundary region. As can be seen, a single precipitate of $Cr_{23}C_6$ on the fusion boundary was observed. The low precipitate density on fusion boundary is most likely due to the high solubility of carbon in the side of B.C.C.–LAS. In addition, the TEM observation also shows that the structure is mainly B.C.C. with lath martensites in LAS side.

Conclusions

The metallographic and crystallographic microstructure, chemical composition, mechanical properties, and orientation relationship in the fusion boundary region of an Alloy 182-A533B-LAS DMW joint were studied. The following conclusions can be drawn from the study.

1. SEM observations revealed the existence of type-II boundary that parallels to the fusion boundary in the DZ of Alloy 182 within a distance of <100 μm. The HAZ near the fusion boundary within a distance of ~400 μm consists of large grains of lath martensite. The microstructure of the HAZ beyond this distance is similar to that of the base metal.
2. The chemical composition transition was found in the narrow zone between the type-II and the fusion boundaries. Highest hardness was also found in this narrow zone, implying a high residual strain level in the narrow zone.
3. The yield strength in HAZ was higher than that of the DZ, weld metal and base metal, which is compatible with the hardness profile across the fusion boundary in the DMW.
4. The orientation relationships at the fusion boundary between the martensite grains in HAZ and the austenite grains in DZ are Bain, K–S, and N–W relationships.
5. The lath martensite was observed in both sides of the type-II boundary in DZ, suggesting the localized

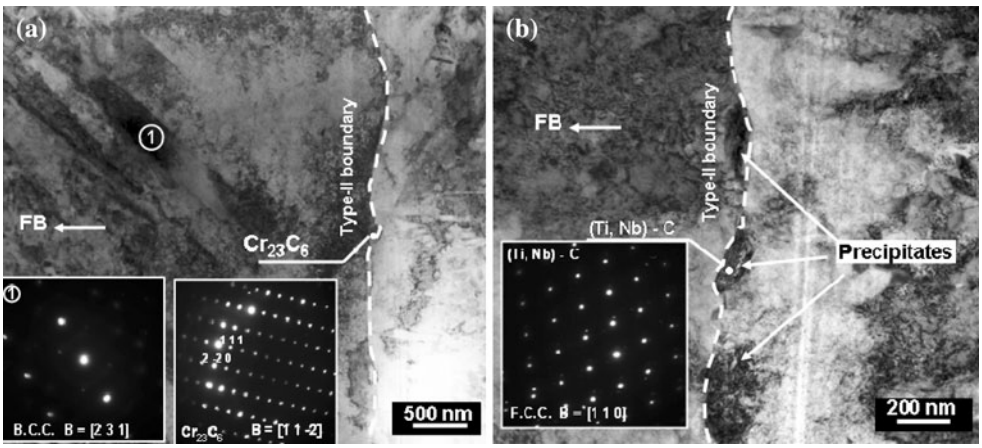

Fig. 10 The TEM observation of the type-II boundary region showing (**a**), the lath martensite adjacent to the type-II boundary and the precipitation of $Cr_{23}C_6$ at the type-II boundary, and (**b**), the precipitation of the composited carbide of Ti/Nb at the type-II boundary

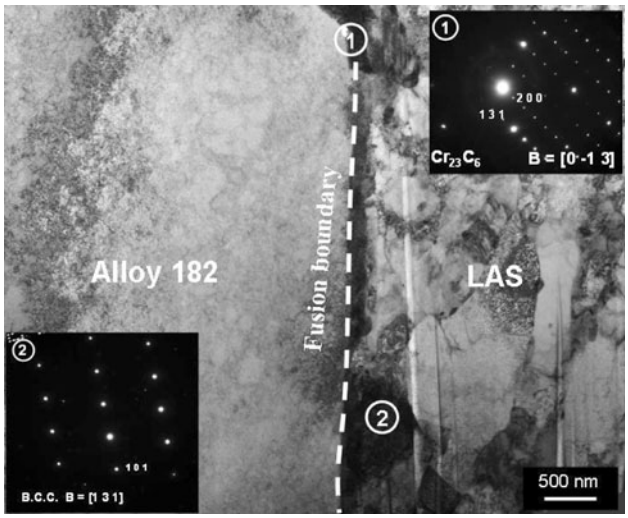

Fig. 11 The TEM observation of the fusion boundary region. While the precipitation of $Cr_{23}C_6$ was observed, the density of the precipitate is low

enrichment of Fe and C in DZ due to the diffusion from LAS to DZ.

6. Composited carbides of Ti and Nb and some $Cr_{23}C_6$ were observed on the type-II boundary. On fusion boundary, however, only a few precipitates of $Cr_{23}C_6$ were observed. The lower precipitate density on the fusion boundary is most likely due to the high solubility of carbon in the side of B.C.C.–LAS.

Acknowledgements This study was supported by a program on "Mechanism of SCC in the Fusion Boundary Zone of Ni-base weld metal and Low Alloy Steel Dissimilar Weld Joints in High Temperature Oxygenated Water" organized by JSCE and sponsored by Japanese BWR utilities. The authors (J. Hou, J. Q. Wang, E.-H. Han, and W. Ke) would thank the Special Funds for the Major State Basic Research Projects G2006CB605000 in China.

References

1. Sireesha M, Albert SK, Shankar V, Sundaresan S (2000) J Nucl Mater 279:65
2. USNRC In: Information Notice 2000-17, 18 October 2000
3. USNRC In: Information Notice 2002-11, 12 March 2002
4. Peng QJ, Shoji T, Yamauchi H, Takeda Y (2007) Corros Sci 49:2767
5. Sakai T, Asami K, Katsumata M, Takada H, Tanaka O (1982) In: 1st international conference on current solutions to hydrogen problems in steels, Washington DC, pp 340–348
6. Matsuda F, Nakagawa H (1984) Trans JWRI 13:159
7. Ohnishi K, Fuji A, Chiba R, Adachi T, Naitoh K, Okada H (1984) Trans Jpn Weld Soc 15:129
8. Kinoshita K, Itoh H, Ebata A, Hattori T (1985) Trans Iron Steel Inst Jpn 25:505
9. Morishige N, Kume R, Okabayashi H (1985) Trans Jpn Weld Soc 16:12
10. Wu Y, Patchett BM (1992) In: 31st metallurgist conference of CIM Edmonton, Canada
11. Nelson TW, Lippold JC, Mills MJ (1998) Sci Technol Weld Join 3:249
12. Nelson TW, Lippold JC, Mills MJ (1999) Weld J 78:329S
13. Nelson TW, Lippold JC, Mills MJ (2000) Weld J 79:267S
14. Lee HT, Jeng SL, Yen CH, Kuo TY (2004) J Nucl Mater 335:59
15. Kim JW, Lee K, Kim JS, Byun TS (2009) J Nucl Mater 384:212
16. Peng Q, Shoji T, Ritter S, Seifert H (2005) In: 12th international conference on environmental degradation of materials in nuclear power systems—water reactors, TMS, pp 589–599
17. Celik A, Alsaran A (1999) Mater Charact 43:311
18. Gourgues AF, Flower HM, Lindley TC (2000) Mater Sci Technol 16:26
19. Morito S, Tanaka H, Konishi R, Furuhara T, Maki T (2003) Acta Mater 51:1789
20. Chilton JM, Barton CJ, Speich GR (1970) J Iron Steel Inst 208:184
21. Krauss G, Marder AR (1971) Metall Trans 2:2343
22. Maki T, Tsuzaki K, Tamura I (1980) Trans Iron Steel Inst Jpn 20:207
23. Morito S, Yoshida H, Maki T, Huang X (2006) Mater Sci Eng A 438:237
24. Pan C, Zhang Z (1996) Mater Charact 36:5
25. Morito S, Huang X, Furuhara T, Maki T, Hansen N (2006) Acta Mater 54:5323